Finite Element Modeling of Gas-Surface Interactions in Hypersonic Flight

John Y. Huang[1], Vincent Casseau[2], Song Gao[3], and Wagdi G. Habashi[4]
CFD Laboratory, Department of Mechanical Engineering, McGill University
Montreal, QC, H3A 2S6, Canada

Accurate numerical simulations of thermal loads during atmospheric re-entry are of paramount importance in the design of space vehicles. The extreme temperatures generated across shocks during re-entry cause gas molecules to dissociate, requiring gas-surface interactions such as atomic recombination reactions to be included in the simulations. This paper describes a module for the simulation of surface catalytic reactions being developed for the hypersonic CFD code, HALO3D (High Altitude Low Orbit 3D), to enhance the accuracy of heat flux predictions. A partially-catalytic model with a constant recombination efficiency is implemented and validated using the Electre test case. A good agreement is found compared to available numerical results and experimental data. This work paves the way for finite-rate surface chemistry and ablation modeling in HALO3D.

I. Introduction

Deployment of small civilian satellites into orbit is a fast-expanding market with many privately-owned space companies venturing into this business. The thrilling successes over the last five years of SpaceX in landing and reusing the first stage of their Falcon 9 orbital rockets have made access to space ever more affordable, with an estimated cost of $2,700 per kilogram put into Low-Earth Orbit (LEO) as of 2018. Their demonstrated capability to deploy many satellites in one launch, known as *rideshare*, is also a major advance. Short rocket turnover time and reuse have become enabling technologies and all other space actors are striving to position themselves in the same market. While some of them are using different rationales, for example the reusable single-stage-to-orbit Skylon spaceplane concept by Reaction Engines Limited or Rocket Lab's battery-powered Electron rocket, the common denominator is the integration of the atmospheric re-entry phase into their designs. Atmospheric re-entry conditions are extreme and reusable Thermal Protection Systems (TPS) made of low-catalytic materials are used to limit atomic recombination at the surface and reduce heat flux. Multi-physics CFD codes are indispensable for fast and reliable aerothermodynamic load predictions along the re-entry trajectory of these hypersonic craft, enabling optimization and improved designs.

The HALO3D CFD code is a comprehensive edge-based parallel finite element (FE) code for the simulation of hypersonic flight. Past developments have been focusing on the implementation of an all-Mach number steady-state Navier–Stokes (NS) solver [1], the modeling of chemical reactions that occur in a non-ionized high-temperature environment [2], and the extension to flows deviating from local thermodynamic equilibrium (LTE) conditions using a two-temperature model [3] and non-equilibrium boundary conditions [4–6]. A magnetohydrodynamics solver is also under development to simulate the effect of imposed and/or induced magnetic field for internal and external flows [7, 8], as well as a Direct Simulation Monte Carlo (DSMC) solver to extend the domain of applicability of HALO3D to the rarefied regime. The present paper is the first step in increasing the capabilities of HALO3D in accounting for surface catalycity, which is key in setting accurate mechanical and thermal requirements in the design of a TPS.

[1] Master student, Department of Mechanical Engineering, 680 Sherbrooke St. West.
[2] Postdoctoral Fellow, Department of Mechanical Engineering, 680 Sherbrooke St. West.
[3] Research and Development Engineer, ANSYS Canada, 1000 Sherbrooke St. West, Suite 2120.
[4] Professor and Director CFD Laboratory, Department of Mechanical Engineering, 680 Sherbrooke St. West.

The high temperature rise across the strong bow shock appearing around hypersonic vehicles causes the dissociation of molecules into atoms, which is an endothermic process. These atomic species are carried through the short shock stand-off distance and may then recombine on the vehicle's surface at different rates, depending on the gas composition, the flow conditions, the surface material, its roughness, and local wall temperature [9]. These reactions, on the other hand, are exothermic; hence surface catalysis affects the gas composition in the vicinity of the surface and therefore the wall heat flux. This phenomenon has been studied since the late 1950s [10–12] and modeled numerically by Tong *et al.* as early as 1973 [13]. Finite-rate surface chemistry has been implemented in various structured and unstructured 3D finite volume codes from the mid-1990's onwards [14–18]. In 2014, a material response module has been coupled to a surface chemistry code and to a flow solver by Farbar *et al.* to accurately simulate the surface thermal and mechanical behavior [19].

The objective of the present work is thus to complement the HALO3D solver with surface catalytic models to be used in conjunction with the other modules. These models are reviewed in Section II, and their numerical formulation in the HALO3D edge-based FE framework is laid out. Verification and validation case scenarios are presented in Section III, and conclusions and future work are listed last in Section IV.

II. Methodology

Common approaches to model surface catalycity are recalled in Section II A. The partially-catalytic surface model implemented in this work and its governing equations and FE formulation are discussed in detail in Section II B. The diffusion model employed in HALO3D and the anisotropic mesh optimization methodology are briefly described in Sections II C and II D, respectively.

A. Gas-Surface Interaction

The five models that are commonly featured in the hypersonic literature are briefly described here:

- the *non-catalytic* model supposes that none of the impinging atoms on the surface are recombining. This model provides the theoretical lower limit for the heat flux;
- the *super-catalytic* model dictates that the species mass fractions on the surface match the free-stream gas composition;
- the *partially-catalytic* model assumes that a given fraction of the impinging atoms recombines on the surface. This recombination efficiency, denoted by γ, may be taken as a constant or be temperature-dependent;
- the *fully-catalytic* model assumes that all impinging atoms recombine on the surface and is therefore related to the partially-catalytic model with $\gamma = 1$. This model provides the theoretical upper limit for the wall heat flux;
- the *finite-rate catalytic* model uses surface reaction kinetics to update the species composition on the surface.

B. Partially-Catalytic Surface

To model the recombination of atomic species s on the surface, the partially-catalytic model assumes a recombination efficiency defined as

$$\gamma_s = \frac{\dot{m}_{\mathrm{rcb},s}}{\dot{m}_{\mathrm{ipg},s}}, \tag{1}$$

where $\dot{m}_{\mathrm{ipg},s}$ and $\dot{m}_{\mathrm{rcb},s}$ are the mass fluxes of the impinging and recombining atoms, respectively, and γ_s is the recombination efficiency of species s. The incident mass flux can be calculated using kinetic theory [20] and is expressed as

$$\dot{m}_{\mathrm{ipg},s} = \rho y_s \sqrt{\frac{R_s T_{\mathrm{w}}}{2\pi}}, \tag{2}$$

in which ρ is the mixture density, y_s is the mass fraction of species s, R_s represents the gas constant of species s, and T_{w} is the wall temperature. The surface production rate of species s per surface area then becomes

$$\dot{\omega}_s = \dot{m}_{\mathrm{rcb},s} = \gamma_s \dot{m}_{\mathrm{ipg},s} = \gamma_s \rho y_s \sqrt{\frac{R_s T_\mathrm{w}}{2\pi}}, \tag{3}$$

For a five-species model (N_2, O_2, N, O, NO), neglecting the recombination of atomic species to form NO on the surface [21] yields the recombination efficiency to be $\boldsymbol{\gamma} = \{+\gamma_N, +\gamma_O, -\gamma_N, -\gamma_O, 0\}^\mathrm{T}$.

1. Species mass balance

For a steady-state compressible viscous gas mixture, the mass conservation of species s on a no-slip, no-penetration, catalytic surface is given by

$$\iiint_V \nabla \cdot \mathbf{J}_s \, \mathrm{d}V = \oiint_S \dot{\omega}_s \, \mathrm{d}S, \tag{4}$$

where $\mathbf{J}_s$ denotes the mass flux of species s. The application of the weak-Galerkin formulation [22] yields the mass balance on the surface to be written as

$$\mathbf{J}_s \cdot \mathbf{n} = \dot{\omega}_s = \rho y_s \gamma_s \sqrt{\frac{R_s T_\mathrm{w}}{2\pi}}, \tag{5}$$

where $\mathbf{n}$ is the unit surface normal vector.

2. Energy balance

For a steady-state compressible viscous gas mixture in the absence of volumetric energy sources, energy dissipation due to the shear stress on the surface, and energy transfer due to radiation, the energy conservation on a no-slip, no-penetration, catalytic surface is given by [16]

$$\oiint_S \left(-\kappa \nabla T + \sum_s^{N_s} h_s \mathbf{J}_s \right) \cdot \mathbf{n} \, \mathrm{d}S = 0, \tag{6}$$

where N_s is the number of species, h_s is the enthalpy of species s, and κ is the mixture thermal conductivity. Substituting the diffusion term with the production term due to recombination yields

$$-\kappa \nabla T \cdot \mathbf{n} = -\sum_s^{N_s} h_s \mathbf{J}_s \cdot \mathbf{n}, \tag{7}$$

$$-\kappa \nabla T \cdot \mathbf{n} = -\sum_s^{N_s} \left(h_s \gamma_s \rho y_s \sqrt{\frac{R_s T_\mathrm{w}}{2\pi}} \right). \tag{8}$$

3. Temperature-dependent recombination efficiency

While a constant recombination efficiency model is enough for simulations where the surface temperature is fixed or barely varying over a body, a temperature dependence ought to be considered otherwise, as γ can increase several folds in just a few hundred kelvins. This change in recombination efficiency has been shown to be adequately described by an Arrhenius law by several authors [22–24] and profiles for species N and O are reported in Figure 1. Scott [23] and Kolodziej and Stewart [24] used arc jet stagnation-point heating rates, whereas Zoby *et al.* [25] derived coefficients for atomic oxygen from the Shuttle Orbiter STS-2 heating rates.

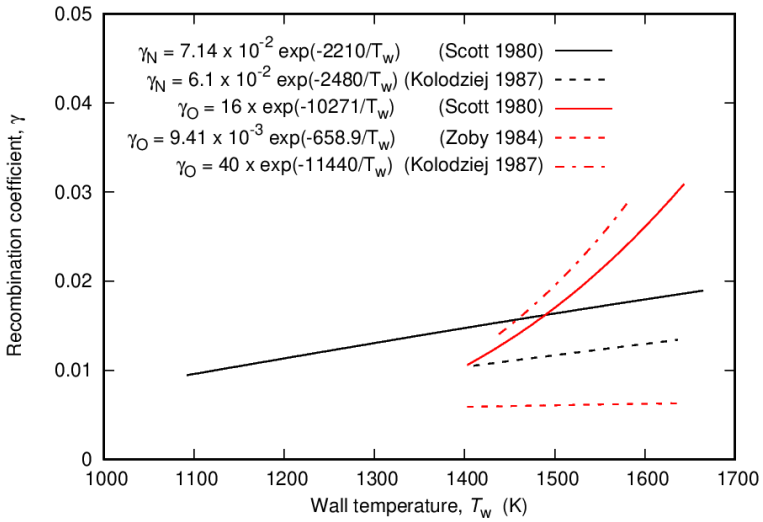

Fig. 1 Evolution of the surface recombination coefficient versus temperature for species N and O.

C. Diffusion Modeling

In HALO3D, the mass flux of species s, $\mathbf{J}_s$, is written according to Fick's law as follows:

$$\mathbf{J}_s = -\rho D \nabla y_s, \tag{9}$$

where D is the diffusion coefficient that is identical to all species composing the gas mixture. In this paper, it is obtained using the Lewis number model such that [26]

$$D = \frac{\mathrm{Le}\kappa}{\rho c_p}, \tag{10}$$

where Le is the Lewis number, and c_p is the mixture heat capacity at constant pressure.

D. Mesh Optimization

An automatic anisotropic mesh optimization code developed by the authors' Lab, OptiGrid [27], that couples solver and mesh during iterations, is used to directionally refine the mesh for the unstructured grid simulations presented in this paper. The directional refinement is achieved through the equi-distribution of the truncation error, defined as the difference between the partial differential equation and its discretized form. While the exact solution is unknown, the error can be estimated using the Hessian matrix, **H**, of a few solution scalar variables chosen based on the nature of the problem being solved. A metric, **M**, based on **H**, is used to define the error estimate in an edge-based fashion as

$$\text{error}\left(\mathbf{x}_i - \mathbf{x}_j\right) = \int_0^1 \sqrt{\left(\mathbf{x}_i - \mathbf{x}_j\right)^{\mathrm{T}} \mathbf{M}(l) \left(\mathbf{x}_i - \mathbf{x}_j\right)}\, dl\,, \tag{11}$$

where $\mathbf{x}_i$ and $\mathbf{x}_j$ are two endpoints of an edge. Letting $\boldsymbol{\Lambda}$ and **R** be the eigenvalues and the right eigenvectors of a combination of the retained solution fields, respectively, **M** and **H** can be written as

$$\mathbf{H} = \mathbf{R}\boldsymbol{\Lambda}\mathbf{R}^{\mathrm{T}}, \tag{12}$$

and

$$\mathbf{M} = \mathbf{R}|\boldsymbol{\Lambda}|\mathbf{R}^{\mathrm{T}}. \tag{13}$$

Refinement, coarsening, node movement and edge swapping are the allowed mesh operations to meet the optimizer's objective to obtain equal edge lengths in metric space, which is synonym to equi-distributing the error estimate in physical space.

III. Results

Verification and validation of the correct implementation of the partially-catalytic boundary conditions for species concentrations and temperature described in Section II are conducted using the Electre test body. Electre is a blunt spherical-conical body with a total length $L = 0.4$ m, a leading-edge radius of 0.035 m, and a cone angle of 4.6 degrees. Electre was tested in two high-enthalpy facilities, namely the ONERA hot-shot F4 and the DLR Stalker tube HEG [28–30]. The locations of the temperature and pressure probes are available in Ref. [31]. The HEG test conditions found in Ref. [32] are recalled in Table 1 and serve as initial and boundary flow conditions for all subsequent simulations.

Table 1 Flow conditions for the Electre test case.

Quantity	Symbol	Value	Unit
Free-stream Mach number	Ma_∞	9.7	-
Free-stream Reynolds number	Re_∞	1.1×10^5	-
Overall Knudsen number	$\mathrm{Kn}_{\mathrm{ov}}$	1.3×10^{-4}	-
Free-stream velocity	U_∞	5,919	$\mathrm{m{\cdot}s^{-1}}$
Free-stream pressure	p_∞	430	Pa
Free-stream temperature	T_∞	790	K
Free-stream N_2 mass fraction	y_{N_2}	0.752	-
Free-stream O_2 mass fraction	y_{O_2}	0.036	-
Free-stream NO mass fraction	y_{NO}	0.033	-
Free-stream N mass fraction	y_N	0	-
Free-stream O mass fraction	y_O	0.179	-
Wall temperature	T_w	300	K

Two grids are utilized to solve the Electre test case. The 95 x 100 x 360 structured mesh shown in Figure 2 with a 90 x 90 patch on the spherical nose is composed of 2.6 M nodes and 2.5 M elements, with a Y^+ value of 0.025 and a geometric progression ratio of 1.1. The mesh presented in Figure 3 is obtained with OptiGrid [27] after four optimization cycles based on density, pressure, temperature, and the velocity components. The initial unstructured mesh contains 340 k nodes and 860 k elements, including 20 prism layers, and a Y^+ value of 0.15 and the same geometric progression ratio. Mesh optimization is conducted on volume and surfaces at the exception of the prism layers on the surface. The adaptation is configured with a 4 M node target and a maximum of 20 M nodes and 40 M elements. The minimum and maximum edge lengths are set to 5×10^{-5} m and 0.3 m, respectively. Within each cycle, twelve adaptation iterations each consisting of one refinement-coarsening operation are sandwiched by 20 and 200 node movements, and then followed by five edge swapping iterations. The final adapted mesh for the fully-catalytic run has 4.1 M nodes and 11.0 M elements.

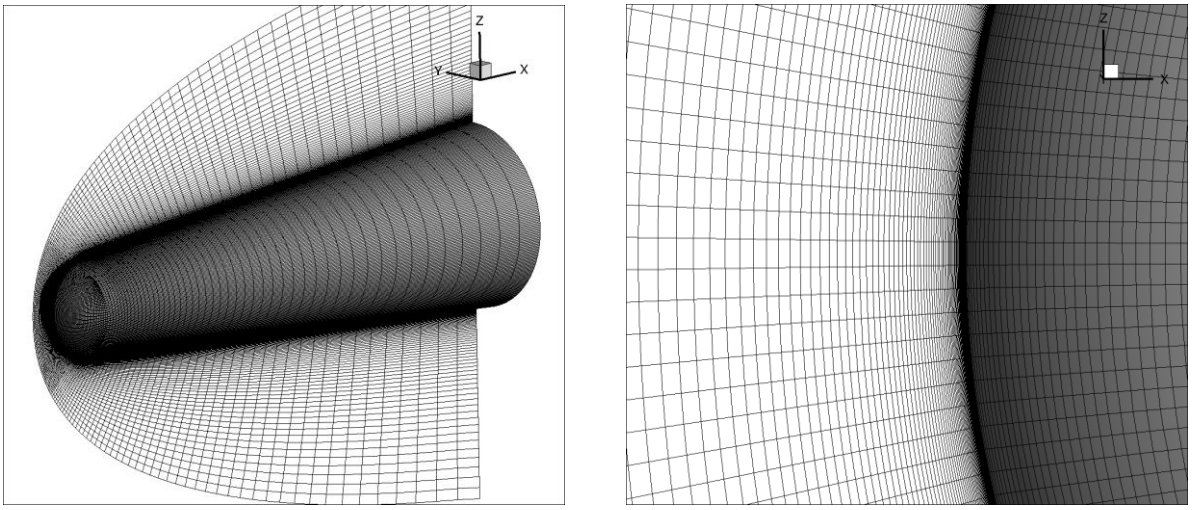

(a) Global view of the mesh **(b) Magnified view of the spherical nose**

Fig. 2 Structured mesh used to simulate the fully-catalytic Electre body.

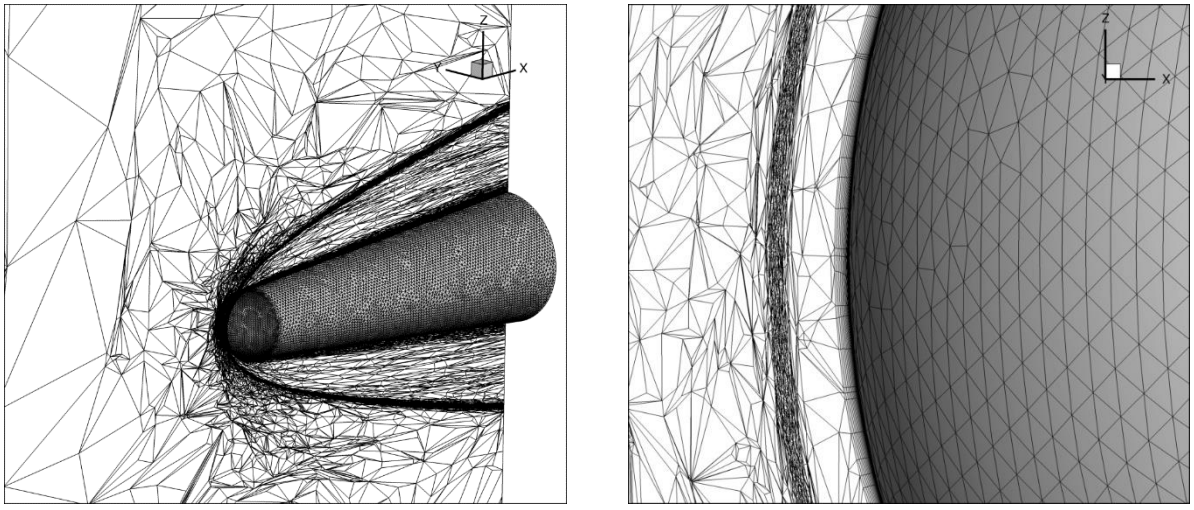

(a) Global view of the mesh **(b) Magnified view of the spherical nose**

Fig. 3 Adapted unstructured mesh used to simulate the fully-catalytic Electre body.

The HALO3D results presented here were obtained with a second-order accurate Roe scheme [33] and the van Albada slope limiter [34]. It is assumed that the flow is in thermal equilibrium, and the thermally perfect gas properties are calculated using polynomials with the National Institute of Standards and Technology (NIST) coefficients [35]. Five species and 17 reactions from Park's 1993 model are considered for volumetric chemistry [36]. Species viscosity and thermal conductivity are derived from Blottner's [37] and Eucken's [38] formulas, respectively, and the mixing rule is that of Wilke [39]. As mentioned in Section II C, a Lewis number of 1.4 is used for the calculation of the diffusion coefficient.

A baseline simulation "*HALO3D nc*" is run using a non-catalytic isothermal wall maintained at a temperature of 300 K. A second simulation labeled as "*HALO3D fc*" employs a fully-catalytic isothermal wall boundary condition, while a third simulation tagged as "*HALO3D pc*" uses a partially-catalytic isothermal wall boundary condition with two constant recombination efficiencies $\gamma_N = \gamma_O = 0.005$ and $\gamma_N = \gamma_O = 0.05$ being employed. The non-catalytic and fully-catalytic simulations are run on both the structured and unstructured meshes, while the partially-catalytic simulation is only performed with the unstructured mesh. For the "*HALO3D nc*" simulation, convergence was achieved after 42.4 hours of computations on the Tournesol high performance computer, using 96 Intel E5-2650 v4

cores running at 2.66 GHz with 1.3 TB of RAM and Intel Omnipath OPA 100 Gb/s Interconnect computer-networking communications.

Contour plots of the *x*-component of the velocity vector and temperature for the structured and unstructured fully-catalytic runs are shown in Figures 4 and 5, respectively. The bow shock for the adapted unstructured grid is better defined than that for the structured grid.

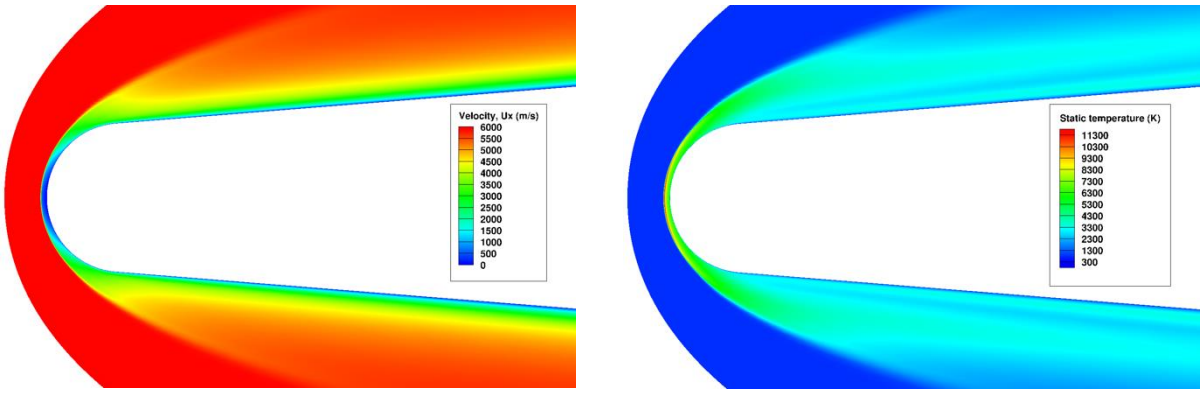

(a) *x*-component of the velocity vector **(b) Temperature**

Fig. 4 Contour plots in the *xz*-plane for the structured fully-catalytic Electre test case.

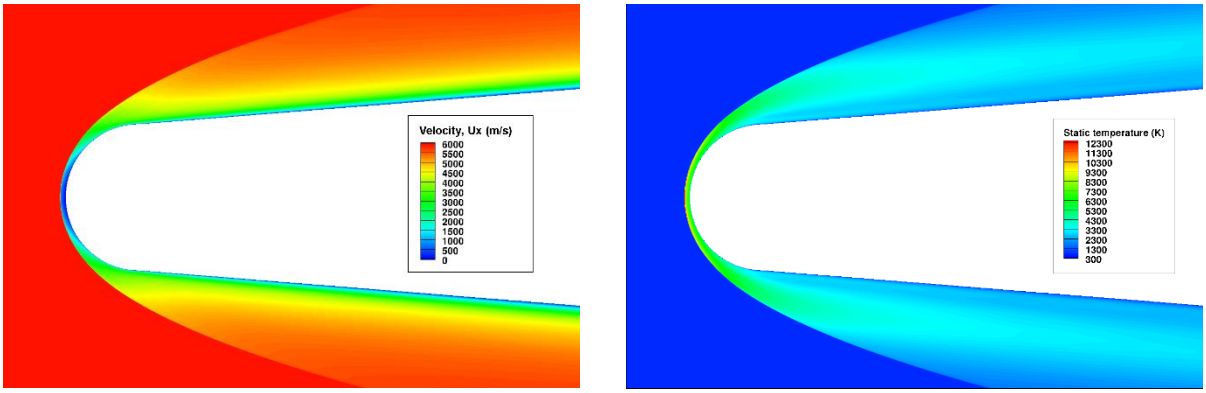

(a) *x*-component of the velocity vector **(b) Temperature**

Fig. 5 Contour plots in the *xz*-plane for the adapted unstructured fully-catalytic Electre test case.

In Figure 6, velocity magnitude, temperature, density, and species mass fractions stagnation line profiles are presented for the unstructured grid. The velocity magnitude, temperature, and mixture density profiles are nearly superimposed for the non-catalytic and super-catalytic cases. Both cases exhibit a shock standoff distance of 2.8 mm, and a maximum temperature of 12,300 K along the stagnation line.

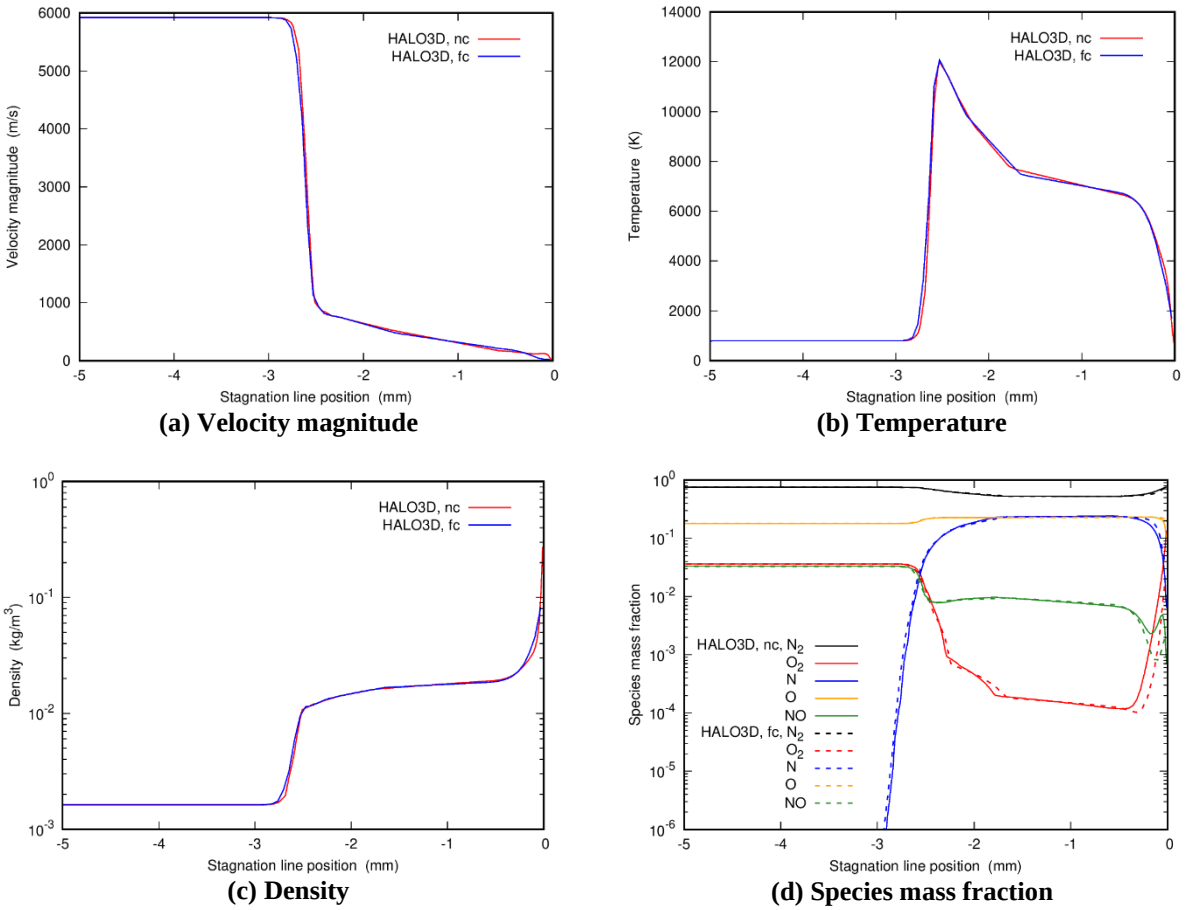

(a) Velocity magnitude **(b) Temperature**

(c) Density **(d) Species mass fraction**

Fig. 6 Stagnation line quantities for the non-catalytic and fully-catalytic unstructured HALO3D runs of the Electre test.

In Figure 7, the surface pressure coefficient and wall heat flux are plotted in the xz-plane as a function of the normalized x-coordinate position. The pressure coefficient profiles for all HALO3D runs are superimposed with the solutions given by Fluent [32]. They are also closely matching the experimental data points on the spherical section and in good concordance on the conical section. As anticipated, the simulation results show that the mesh type and surface chemistry do not have a significant influence on the pressure coefficient.

The fully-catalytic heat flux profiles for the unstructured HALO3D simulation and the Fluent run are in good agreement, but they predict slightly higher wall heat fluxes than the experimental results. The HALO3D heat flux profiles for the partially-catalytic runs are bounded by the fully-catalytic and non-catalytic curves, and the values of the recombination efficiencies, $\gamma_N = \gamma_O = 0.005$ and $\gamma_N = \gamma_O = 0.05$, are shown to tightly bracket experimental results. The surface heat flux is improved because of the enhanced shock capturing presented in Figure 4, therefore illustrating the benefit of using an anisotropic mesh optimization tool for accurate heat flux predictions.

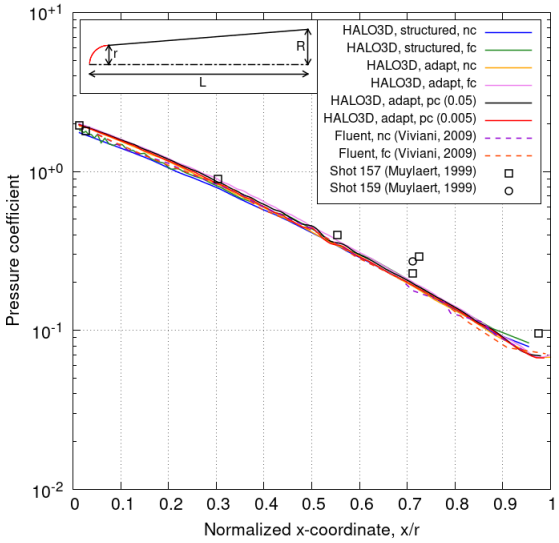

(a) Pressure coefficient on the spherical section

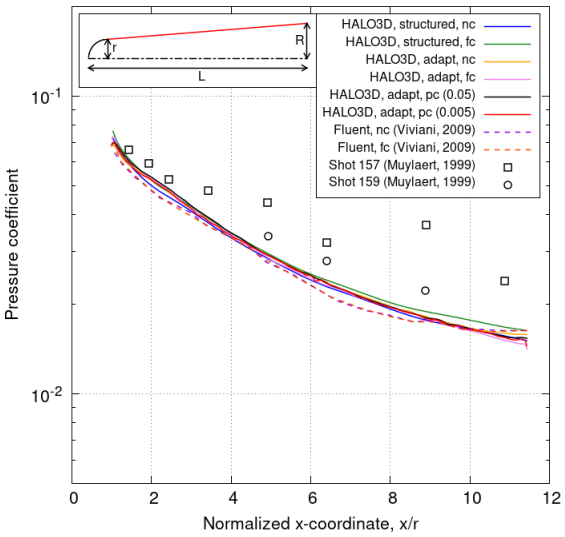

(b) Pressure coefficient on the conical section

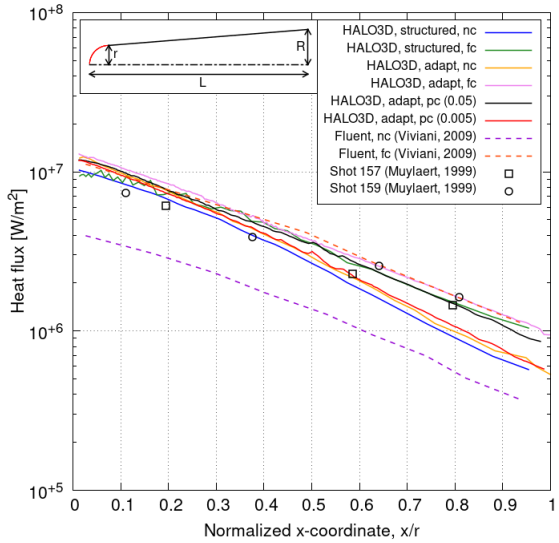

(c) Wall heat flux on the spherical section

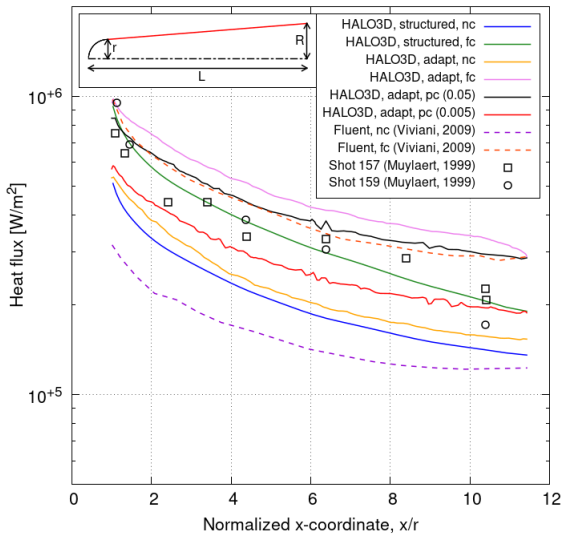

(d) Wall heat flux on the conical section

Fig. 7 Surface quantities for the Electre test case.

IV. Conclusion

As part of a continuous effort to create a single code, HALO3D, that can simulate the conditions of the entire trajectory of a hypersonic re-entry vehicle, this paper emphasizes the developments of a gas-surface interactions module. A fully-catalytic wall boundary condition has been implemented and verified with previously published numerical results using the Electre body. The use of an unstructured grid in conjunction with the anisotropic mesh optimizer OptiGrid, aligning the element edges with the characteristic flow features, has exhibited less numerical diffusion, a sharper shock, and less spurious oscillations in the heat flux profile compared to the structured run. Subsequently, a partially-catalytic model has been introduced and the solutions for $\gamma_N = \gamma_O = 0.005$ and $\gamma_N = \gamma_O = 0.05$ have been shown to closely bracket the experimental data.

Work is being directed towards the introduction of temperature-dependent recombination efficiencies using a surface energy balance boundary condition and the implementation of finite-rate surface chemistry.

Acknowledgments

The CFD Lab extends its thanks to the Lockheed Martin Corporation, ANSYS Canada, and MITACS for the MITACS Accelerate grant supporting the current work.

References

[1] Gao, S., Habashi, W. G., Isola, D., Baruzzi, G. S., and Fossati, M., "A Jacobian-free Edge-based Galerkin Formulation for Compressible Flows," *Computers & Fluids*, vol. 143, no. 1, 2016, pp. 141–156.

[2] Seguin, J., Gao, S., Habashi, W. G., Isola, D., and Baruzzi, G. S., "A Finite Element Solver for Hypersonic Flows in Thermo-Chemical Non-Equilibrium, Part I," *International Journal of Numerical Methods for Heat & Fluid Flow*, 2019.

[3] Park, C., *Nonequilibrium Hypersonic Aerothermodynamics*, Wiley International, New York, 1990.

[4] Maxwell, J. C., "VII. On Stresses in Rarified Gases Arising from Inequalities of Temperature," *Philosophical Transactions of the Royal Society of London*, vol. 170, no. 1, 1879, pp. 231–256.

[5] Smoluchowski, M. R., "Über Wärmeleitung in verdünnten Gasen," *Annalen der Physik*, vol. 300, no. 1, 1898, pp. 101–130.

[6] Dumas, M.-E., Habashi, W. G., Baruzzi, G. S., Isola, D., and Fossati, M., "Finite Element Modeling of Nonequilibrium Fluid-Wall Interaction at High-Mach Regime," *Journal of Aircraft*, vol. 54, no. 6, 2017, pp. 2330–2339.

[7] Zhang, W., Habashi, W. G., Salah, N. B., Isola, D., and Baruzzi, G. S., "Edge-Based Finite Element Formulation of Hypersonic Flows Under an Imposed Magnetic Field," *AIAA Journal*, vol. 56, no. 7, 2018, pp. 2756–2768.

[8] Zhang, W., Habashi, W. G., Salah, N. B., Isola, D., and Baruzzi, G. S., "Edge-Based Finite Element Modeling of Magnetogasdynamic-Based Propulsion Systems," *AIAA Journal*, vol. 57, no. 7, 2019, pp. 3003–3013.

[9] Zuppardi, G. and Verde, G., "An approximate method to evaluate the surface catalycity in high enthalpy flows", *Transactions on Modelling and Simulation*, vol. 16, no. 1, 1997, pp. 589–598.

[10] Fay, A. J. and Ridell, F. R., "Theory of Stagnation Point Heat Transfer in Dissociated Air," *Journal of the Aeronautical Sciences*, vol. 28, no. 1, 1958, pp. 73–122.

[11] Goulard, R., "On Catalytic Recombination Rates in Hypersonic Stagnation Heat Transfer," *Jet Propulsion*, vol. 28, no. 1, 1958, pp. 737–745.

[12] Inger, G. R., "Nonequilibrium Stagnation Point Boundary Layers with Arbitrary Surface Catalycity," *AIAA Journal*, vol. 1, no. 8, 1963, pp. 1776–1784.

[13] Tong, H., Buckingham, A. C., and Morse, H. L., "Nonequilibrium Chemistry Boundary Layer Integral Matrix Procedure," *NASA*, NTRS 19730023103, 1973.

[14] Miller, J. H., Tannehill, J. C., Wadawadigi, G., Edwards, T. A., and Lawrence, S. L., "Computation of Hypersonic Flows with Finite Catalytic Walls," *Journal of Thermophysics and Heat Transfer*, vol. 9, no. 3, 1995, pp. 486–493.

[15] Valentini, P., Schwartzentruber, T. E., and Cozmuta, I., "A Mechanism-Based Finite-Rate Surface Catalysis Model for Simulating Reacting Flows," *Journal of Heat Transfer*, vol. 117, no. 1, 2009, pp. 495–501.

[16] Marschall, J. and Maclean, M., "Finite-Rate Surface Chemistry Model, I: Formulation and Reaction System Examples," *42nd AIAA Thermophysics Conference*, AIAA Paper 2011-3783, 2011.

[17] Maclean, M., Marschall, J., and Driver D. M., "Finite-Rate Surface Chemistry Model, II: Coupling to Viscous Navier–Stokes Code," *42nd AIAA Thermophysics Conference*, AIAA Paper 2011-3784, 2011.

[18] Alkandry, H., Farbar, E., and Boyd, I. D., "Evaluation of Finite-Rate Surface Chemistry Models for Simulation of the Stardust Reentry Capsule," *43rd AIAA Thermophysics Conference*, AIAA Paper 2012-2874, 2012.

[19] Farbar, E., Alkandry, H., Wiebenga, J., and Boyd, I. D., "Simulation of Ablating Hypersonic Vehicles with Finite-Rate Surface Chemistry," *11th AIAA/ASME Joint Thermophysics and Heat Transfer Conference*, AIAA Paper 2014-2124, 2014.

[20] Maxwell, J. C., "V. Illustrations of the Dynamical Theory of Gases. Part I. On the Motions and Collisions of Perfectly Elastic Spheres," *The London, Edinburgh, and Dublin Philosophical Magazine and Journal of Science*, vol. 19, no. 124, 1860, pp. 19–32.

[21] Barbato, M., Giordano, D., and Bruno, C., "Comparison between Finite Rate and Other Catalytic Boundary Conditions for Hypersonic Flows," *6th AIAA/ASME Joint Thermalphysics and Heat Transfer Conference*, 1994.

[22] Zienkiewicz, O. C., Taylor, R. L., and Zhu, J. Z., *The Finite Element Method: Its Basics and Fundamentals*, Elsevier, 2005.

[23] Scott, C. D., "Catalytic Recombination of Nitrogen and Oxygen on High-Temperature Reusable Surface Insulation," *15th AIAA Thermophysics Conference*, AIAA Paper 1980-1477, 1980.

[24] Kolodziej, P. and Stewart, D. A., "Nitrogen Recombination on High-Temperature Reusable Surface Insulation and the Analysis of its Effect on Surface Catalysis," *22nd AIAA Thermophysics Conference*, AIAA Paper 1987-1637, 1987.

[25] Zoby, E. V., Gupta, R. N., and Simmonds, A. L., "Temperature-Dependent Reaction-Rate Expression for Oxygen Recombination at Shuttle Entry Conditions," *22nd AIAA Aerospace Sciences Meeting*, AIAA Paper 1984-224, 1984.

[26] Candler, G. V. and Nompelis, I., "Computational Fluid Dynamics for Atmospheric Entry," *RTO-AVT-VKI Lecture Series*, 2009-AVT-162, 2009

[27] Habashi, W. G., Dompierre, J., Bourgault, Y., Fortin, M., and Vallet, M.-G., "Certifiable Computational Fluid Dynamics Through Mesh Optimization, Special Issue on Credible Computational Fluid Dynamics Simulation", *AIAA Journal*, vol. 36, no. 5, 1998, pp. 703–711.

[28] Walpot, L. and Kordulla, W., "Synthesis of the Electre in the Hypersonic Impulse Facility HEG," *Proc. of the Aerothermodynamics Workshop*, ESTEC, Noordwijk, The Netherlands, 1996.

[29] Sagnier, P. and Vérant, J.-L., "Flow Characterization in the ONERA F4 High-Enthalpy Wind Tunnel," *AIAA Journal*, vol. 36, no. 4, 1998, pp. 522–531.
[30] Muylaert, J., Walpot, L., and Vennemann, D., "A Review of European Code-Validation Studies in High-Enthalpy Flow," *Philosophical Transactions of the Royal Society of London. Series A: Mathematical, Physical and Engineering Sciences*, vol. 357, no. 1759, 1999, pp. 2249–2278.
[31] Durand, G., Schwane, R., and Muylaert, J., "ESA Manned Space Transportation Programme," *Proc. of the Aerothermodynamics Workshop*, YPA/2254/JM, 1997.
[32] Viviani, A. and Pezzella, G., "Nonequilibrium Aerothermodynamics for a Capsule Reentry Vehicle," *Engineering Applications of Computational Fluid Mechanics*, vol. 3, no. 4, 2009, pp. 543–561.
[33] Roe, P. L., "Approximate Riemann Solvers, Parameter Vectors, and Difference Schemes," *Journal of Computational Physics*, vol. 43, no. 2, 1981, pp. 357–372.
[34] Venkatakrishnan, V., "Convergence to Steady State Solutions of the Euler Equations on Unstructured Grids with Limiters," *Journal of Computational Physics*, vol. 118, no. 1, 1995, pp. 120–130.
[35] Linstrom, P. J., "NIST Chemistry WebBook, SRD 69," *National Institute of Standards and Technology Standard Reference Database* [online database], URL: https://webbook.nist.gov/chemistry/ [retrieved 26 January 2020]
[36] Park, C., "Review of Chemical-Kinetic Problems of Future NASA Missions, I: Earth Entries," *Journal of Thermophysics and Heat Transfer*, vol. 7, no. 3, 1993, pp. 385–398.
[37] Blottner, F. G., Johnson, M., and Ellis, M., "Chemically Reacting Viscous Flow Program for Multi-Component Gas Mixtures," *Sandia Laboratories Report*, NO. SC-RR-70-754, Albuquerque, New Mexico, 1971.
[38] Vincenti, W. G. and Kruger, C. H., *Introduction to Physical Gas Dynamics*, Krieger Publishing Company, Malabar, Florida, 1965.
[39] Wilke, C. R., "A Viscosity Equation for Gas Mixtures," *The Journal of Chemical Physics*, vol. 18, no. 4, 1950, pp. 517–519.